

Original article

Activation of LAMP1-mediated lipophagy by sulforaphane inhibits cellular senescence and intervertebral disc degeneration

Tianyu Qin^{a,b,c,1}, Ming Shi^{d,e,1}, Yongheng Xie^{a,c,1}, Naibo Feng^{a,c}, Chungeng Liu^{a,c},
Ke Chen^{a,c}, Yining Chen^{a,c}, Wanli Zheng^d, Mingxi Zhu^d, Songlin Peng^{a,c,g,*},
Guozhi Xiao^{c,f,**}, Houqing Long^{a,c,g,***}

^a Division of Spine, Department of Orthopedic Surgery, Shenzhen People's Hospital, The Second Clinical Medical College, Jinan University, Shenzhen, 518020, Guangdong, China

^b Integrated Chinese and Western Medicine Postdoctoral Research Station, Jinan University, Guangzhou, 510632, Guangdong, China

^c Shenzhen Key Laboratory of Musculoskeletal Tissue Reconstruction and Function Restoration, Shenzhen, 518020, Guangdong, China

^d Department of Orthopedics, The Eighth Affiliated Hospital of Sun Yat-sen University, Shenzhen, 528406, Guangdong, China

^e Department of Orthopedic, Zibo Central Hospital, Zibo, 255000, Shandong, China

^f Department of Biochemistry, Shenzhen Key Laboratory of Cell Microenvironment, School of Medicine, Southern University of Science and Technology, Shenzhen, 518055, Guangdong, China

^g Shenzhen Clinical Research Centre for Geriatrics, Shenzhen People's Hospital, Shenzhen, 518020, Guangdong, China



A B S T R A C T

Background: Intervertebral disc degeneration (IDD) is a major cause of chronic low back pain, involving lipid dysregulation and cellular senescence in nucleus pulposus (NP) cells. However, the relationship between lipid accumulation and cellular senescence in IDD remain unclear. This study aims to investigate whether lipid accumulation promotes NP cell senescence and explore the role of LAMP1-mediated lipophagy in mitigating these effects.

Methods: Human and rat NP tissue samples were analyzed for lipid levels and senescence markers, including p16, p21 and p53. NP cells were treated with palmitic acid (PA) to induce lipid accumulation. Multi-omics analysis and machine learning were used to identify LAMP1 as a key regulator of lipid metabolism in NP cells. The effects of LAMP1 overexpression on lipid clearance and cellular senescence were evaluated in vitro. The natural compound sulforaphane (SFN) was applied to stimulate LAMP1-mediated lipophagy. LAMP1 knockdown was used to assess the role of LAMP1 in SFN-induced lipophagy and its impact on lipid accumulation and senescence. In vivo, SFN treatment was administered to rats with IDD induced by needle puncture. MRI, X-ray, and histological analysis were performed to evaluate the effects of SFN on disc degeneration, lipid accumulation, and senescence in NP tissue.

Results: Excessive lipid accumulation in degenerated NP tissues was observed, along with increased expression of senescence markers. Further experiments demonstrated that LAMP1 overexpression reduced lipid accumulation and senescence in NP cells. Notably, the natural compound sulforaphane enhanced LAMP1-mediated lipophagy, promoting lipid clearance and reducing senescence. In vivo, sulforaphane treatment in a rat IDD model reduced lipid accumulation and delayed IDD.

Conclusion: Our findings suggest that LAMP1-mediated lipophagy plays a crucial role in inhibiting NP cell senescence and that sulforaphane can slow the progression of IDD by activating LAMP1.

The translational potential of this article: This study indicates that the therapeutic effects of sulforaphane in mitigating lipid accumulation and senescence can provide an effective treatment strategy for delaying the progression of IDD in the future.

1. Introduction

Low back pain (LBP) is a prevalent global public health issue and is

one of the leading causes of disability and economic burden. An estimated 568.4 million people worldwide are affected by LBP [1]. In the United States, LBP was the top healthcare expenditure among 154 health

* Corresponding author. Division of Spine, Department of Orthopedic Surgery, Shenzhen People's Hospital, The Second Clinical Medical College, Jinan University, Shenzhen, 518020, Guangdong, China.

** Corresponding author. Shenzhen Key Laboratory of Musculoskeletal Tissue Reconstruction and Function Restoration, Shenzhen, 518020, Guangdong, China.

*** Corresponding author. Division of Spine, Department of Orthopedic Surgery, Shenzhen People's Hospital, The Second Clinical Medical College, Jinan University, Shenzhen, 518020, Guangdong, China.

E-mail addresses: pengsonglin@mail.sustech.edu.cn (S. Peng), xiaogz@sustech.edu.cn (G. Xiao), houqinglong@163.com (H. Long).

¹ These authors contributed equally to this work.

conditions in 2016, incurring costs totaling approximately \$134.5 billion [2]. Intervertebral disc degeneration (IDD) is recognized as one of the primary causes of LBP. As people age, the severity of IDD increases, which contributes to the varying prevalence of LBP across age groups [1,3]. IDD is a complex, multifactorial process involving mechanical stress, oxidative stress, and metabolic disorders [4–6]. The nucleus pulposus (NP), the core component of the intervertebral disc, plays a central role in IDD. Degeneration of NP tissue is not only a hallmark of IDD pathology but is also closely influenced by multiple intracellular and extracellular factors [7,8]. Nevertheless, the exact pathophysiological mechanisms of IDD remain unclear, presenting challenges in developing effective therapeutic strategies.

Lipid metabolism disorders are characterized by abnormalities in lipid synthesis, transport, or utilization, resulting in lipid accumulation or abnormal distribution in tissues [9]. Numerous studies have established a strong link between lipid metabolism disorders and various degenerative diseases, such as osteoarthritis, osteoporosis, age-related macular degeneration, and Alzheimer's disease [10–13]. Recently, interest has grown regarding a potential connection between lipid metabolism disorders and IDD. Clinical studies have shown that elevated serum levels of cholesterol, triglycerides, and low-density lipoprotein (LDL) cholesterol are significantly associated with IDD and are recognized as independent risk factors for this condition [14,15]. Supporting these findings, animal studies have demonstrated that high-fat diets in mice and rats can exacerbate IDD [16,17]. Moreover, triglyceride and cholesterol accumulation has been detected in the NP tissue of degenerated discs, providing additional evidence for the role of lipid accumulation in IDD [17,18].

Despite this accumulating evidence, conflicting findings challenge the consistency of this association. For example, Keser et al. reported no significant correlation between blood lipid levels and lumbar disc herniation caused by IDD [19]. Meanwhile, animal study has found no signs of disc degeneration in mice fed high-fat diets, although changes in bone structure were observed [20,21]. Metabolomic analyses have further shown that lipid levels—including fatty acids, triglycerides, and cholesterol—are significantly lower in degenerated discs compared to healthy ones [22]. Consequently, the precise relationship between lipid metabolism disorders and IDD remains inconclusive and warrants further studies.

Cellular senescence is an irreversible arrest of the cell cycle triggered by various stressors, including DNA damage, oxidative stress, and chemotherapeutic drug toxicity [23]. As cells age, their efficiency in lipid metabolism declines, particularly in fatty acid oxidation, autophagy, and mitochondrial function. These impairments reduce the cells' ability to utilize or degrade lipids, leading to lipid accumulation within cells and tissues [24–26]. Furthermore, lipid synthesis pathways become significantly upregulated in senescent cells, often linked to the increased activity of sterol regulatory element-binding protein 1 (SREBP1) [27]. This excessive lipid accumulation causes lipotoxicity, which induces cellular stress, oxidative stress, and inflammatory responses, ultimately accelerating cellular aging and functional decline [9,28]. This establishes a vicious cycle: lipid accumulation promotes cellular senescence, which further exacerbates lipid buildup.

NP cell senescence plays a critical role in the progression of intervertebral disc degeneration. Senescent NP cells release senescence-associated secretory phenotype (SASP) factors, leading to chronic inflammation, matrix degradation, and cellular dysfunction, thereby accelerating disc degeneration [29,30]. Therefore, exploring the connection between lipid metabolism and cellular senescence offers valuable insights into the core mechanisms of IDD and provides scientific support for developing new therapeutic and preventive strategies.

In this study, we observed significant lipid accumulation and cellular senescence in the NP tissue of both human and rat degenerated discs. Moreover, lipid accumulation was found to promote NP cell senescence. Through single-cell sequencing, transcriptome analysis, and machine learning algorithms, we identified lysosome-associated membrane

protein 1 (LAMP1) as a key regulator of lipid metabolism in NP cells. LAMP1 overexpression effectively reduced lipid accumulation and cellular senescence in NP cells. Furthermore, we found that the natural compound sulforaphane (SFN) enhances LAMP1-mediated lipophagy, thereby slowing IDD progression. This research provides new insights into the roles of lipid metabolism and cellular senescence in IDD. By promoting LAMP1-mediated lipophagy, SFN offers a promising strategy for mitigating IDD and improving clinical outcomes for patients with LBP.

2. Materials and methods

2.1. Patient samples

This study included 20 patients, from whom 20 NP tissue samples were collected. The patients, aged between 13 and 75 years, consisted of 7 females and 13 males. These individuals underwent spinal surgery between 2021 and 2024. During the procedures, the NP tissue was obtained by posterior approach, dissecting the AF tissue and using specialized instruments. Some tissue samples were fixed with 4 % paraformaldehyde for histological staining, while others were rapidly stored at -80°C for subsequent metabolic analyses, such as triglyceride detection. Preoperative T2-weighted MRI scans were used to assess the degree of IDD, categorized using the Pfirrmann grading system. The study was approved by the Ethics Committee of Shenzhen People's Hospital.

2.2. NP cell isolation and culture

For rat NP cell extraction, NP tissues were collected after euthanasia by intraperitoneal injection of pentobarbital. The tail was removed, the skin was dissected, and the Co7/Co8 intervertebral discs were exposed. After incising the AF, NP tissue was extracted with forceps and immediately immersed in DMEM with 10 % FBS. It underwent two-step enzymatic digestion: protease treatment at 37°C for 45 min, followed by centrifugation at 1000 rpm for 5 min. The pellet was resuspended in DMEM and digested with type II collagenase for 15 min at 37°C . Cells were cultured in DMEM with 10 % FBS and 1 % penicillin-streptomycin. For human NP cell extraction, NP tissues from spinal surgery were washed, minced, and digested with 0.2 % collagenase II at 37°C for 4–6 h. After filtration and centrifugation, cells were resuspended in DMEM with 10 % FBS and 1 % penicillin-streptomycin for culture.

2.3. Transmission electron microscopy

After treatment, NP cells were trypsinized, collected into pellets, and fixed overnight at 4°C in 2.5 % glutaraldehyde. The fixed cells were washed with PBS and post-fixed with 1 % osmium tetroxide at 4°C for 2 h. After washing with buffer, the samples were dehydrated using a graded ethanol series and embedded in Epon 812. Ultrathin sections were prepared using a Leica UC7 ultramicrotome. These sections were post-stained with uranyl acetate for 20 min and lead citrate for 12 min to enhance contrast. Finally, lipid droplets within the cells were visualized and analyzed using a Tecnai G2 Spirit transmission electron microscope (FEI, USA).

2.4. Triglyceride assay

The intracellular Triglyceride level was assayed using a triglyceride assay kit (BC0625, Solarbio, China). NP tissues were homogenized on ice with extraction reagent (n-heptane/isopropanol, 1:1) at a 1:10 ratios. The homogenate was centrifuged at 8000 g for 10 min at 4°C , and the supernatant was collected. NP cells were treated similarly, with ultrasonic disruption, followed by centrifugation. Triglycerides were extracted and saponified with potassium hydroxide, releasing glycerol and fatty acids. Glycerol was oxidized by periodic acid to form

formaldehyde, which reacted with acetylacetone to produce a yellow compound measured at 420 nm. All reactions occurred in a 65 °C water bath, with samples diluted as needed.

2.5. Cholesterol assay

The intracellular cholesterol level was assayed using a cholesterol assay kit (STA-384, Cell Biolabs, United States). NP cells were digested with trypsin, resuspended in PBS, and centrifuged. After discarding PBS, chloroform, isopropanol, and ethyl phenyl polyethylene glycol (EPEG) were added, followed by grinding with magnetic beads and extraction. NP tissue underwent the same process. Samples were dried at 60 °C and vacuum-dried to yield cholesterol crystals. Crystals were dissolved in assay diluent. A reaction mixture with cholesterol oxidase, HRP, colorimetric probe, and esterase was added to a 96-well plate and incubated at 37 °C for 45 min. Absorbance at 540–570 nm was measured, and cholesterol ester content was calculated by subtracting free cholesterol from total cholesterol.

2.6. Fluorescent detection of LDs

After washing with PBS, cells were incubated with a staining solution containing either Nile Red or BODIPY 493/503 dye, following the manufacturer's protocol (Beyotime, China). Typically, 1 mL of staining solution was added per well in a 6-well plate, and incubation was performed at room temperature for 10–20 min, protected from light. After incubation, cells were washed with PBS to remove excess dye. Fluorescence microscopy was used to detect LDs, with excitation/emission wavelengths set to 488/510 nm for BODIPY 493/503 or 552/636 nm for Nile Red.

2.7. β -gal staining

After treatment, cells were washed with PBS and fixed with β -galactosidase fixative solution for 15 min at room temperature. Following fixation, the cells were washed three times with PBS, and 1 mL of staining solution, prepared according to the kit instructions (Beyotime, China), was added to each well. Cells were incubated at 37 °C overnight, avoiding CO₂ incubators. The next day, stained cells were observed under an optical microscope.

2.8. EdU assay

Cells were incubated with 10 μ M EdU solution for 2 h at 37 °C. After removing the medium, cells were fixed with 4 % paraformaldehyde for 15 min and permeabilized with 0.3 % Triton X-100 for 10 min. A Click reaction mixture with fluorescent azide, CuSO₄, and additive was prepared according to the kit instructions (Beyotime, China) and applied for 30 min at room temperature, protected from light. After washing with PBS, cells were counterstained with DAPI and analyzed using a fluorescence microscope.

2.9. Cell cycle

Cells were fixed in 70 % ethanol at 4 °C for at least 30 min, then centrifuged at 1000 g for 5 min and washed with PBS. A staining solution with propidium iodide (PI) and RNase A was prepared according to the kit instructions (MCE, USA). Cells were resuspended in 500 μ L of the solution and incubated at 37 °C for 30 min, protected from light. Flow cytometry was used to analyze the stained cells at an excitation wavelength of 488 nm to measure red fluorescence and determine DNA content.

2.10. CCK-8

NP cells were seeded into 96-well plates at a density of 2000 cells per

well in 100 μ L of culture medium. After treatment, CCK-8 reagent (APExBIO, USA) was added to each well and incubated at 37 °C. Absorbance was measured at 450 nm using a microplate reader. The intensity of the color formed is directly proportional to the number of viable cells, allowing for the assessment of cell proliferation or cytotoxicity.

2.11. Co-immunoprecipitation

Cells were lysed with IP lysis buffer (Beyotime, China) containing a protease inhibitor cocktail and incubated for 20 min. After centrifugation at 12,000 rpm for 10 min at 4 °C, the supernatants were collected. Primary antibodies against LAMP1 (Santa Cruz, sc-20011, USA) and LC3 (Proteintech, 14600-1-AP, USA) were added to the supernatants, and the mixture was rotated overnight at 4 °C. Magnetic beads were incubated with the complexes for 2 h at room temperature. After three washes with IP washing buffer, the immunoprecipitants were eluted by boiling in 1 \times SDS-loading buffer for 10 min for further analysis via Western blot.

2.12. Animal studies

All animal experiments were approved by the Institutional Animal Care and Use Committee of Shenzhen People's Hospital. Twenty-four male SD rats (12 weeks old, 200–250 g) were randomly divided into three groups: Sham, IDD, and SFN. Anesthesia was administered via intraperitoneal injection of 2 % pentobarbital. For IDD induction, a 20G needle was inserted into the Co7/8 intervertebral disc, rotated 360° clockwise, and held for 30 s. In the SFN group, 5 μ M SFN (MCE, USA) was injected into the disc using a 34G Hamilton syringe, with injections performed weekly for four weeks. After four weeks, MRI and X-ray of the caudal vertebrae were conducted.

2.13. Bioinformatics analysis

Data were retrieved from the GEO database (<https://www.ncbi.nlm.nih.gov/geo/>). GSE205535 provided two samples (one control and one IDD case) for single-cell analysis, while GSE186542 and GSE245147 each contained expression profiles from six patients (three controls and three IDD cases). Single-cell analysis was conducted using the Seurat package to filter low-quality cells and remove doublets with Doublet-Finder, followed by normalization, PCA, and UMAP for dimensionality reduction and cluster visualization. Clusters were annotated using the CellMarker database and literature. Metascape was employed for GO enrichment analysis of lipid metabolism-related genes. Feature selection was performed using Lasso logistic regression and random forest algorithms with the “glmnet” package, selecting the top 10 features by % IncMSE. GSVA further evaluated pathway-level changes using gene sets from the Molecular Signatures Database. All statistical analyses were conducted in R (version 4.3.2), with $p < 0.05$ indicating statistical significance.

2.14. Statistical analysis

GraphPad Prism 9.0 software was utilized for all statistical assessments, with P-values less than 0.05 considered statistically significant. Each experiment was performed with at least three biological replicates. The Shapiro–Wilk test was used to check whether the data conform to the normal distribution. Data consistent with normal distribution are shown as mean \pm SD. Student's t-test was performed to test the differences between two groups. One-way ANOVA was performed for comparisons among three or more groups. Correlations between variables were examined through linear regression analysis.

A detailed description of additional materials and methods can be found in the Supplemental data.

3. Results

3.1. Lipid accumulation in degenerated NP tissue and its association with senescence

To investigate the relationship between lipid metabolism disorders and IDD, we collected human NP samples with varying degeneration levels based on the Pfirrmann grading system (Fig. 1A). We measured triglyceride and cholesteryl ester levels within the NP tissue, finding that these levels were lower in mildly degenerated samples compared to severely degenerated ones (Fig. 1B and C). Lipid droplets (LDs), intracellular lipid storage structures, are enclosed by a phospholipid monolayer membrane with associated proteins, notably PLIN2 (Perilipin 2), a key LD-associated protein (Fig. 1D). Transmission electron microscopy (TEM) analysis showed an increased number of LDs in severely degenerated NP tissue (Fig. 1E). Immunohistochemical (IHC) analysis further demonstrated a significant increase in PLIN2 expression and senescence markers (p21 and p16) in the severely degenerated group, and PLIN2 expression was positively correlated with the expression of p21 and p16 (Fig. 1F–H and Fig. S1A–E). Consistently, western blot (WB) results indicated that the protein levels of PLIN2, p16, and p21 increased with IDD severity (Fig. S1F).

Next, we established an IDD model in Sprague–Dawley (SD) rats (Fig. 1I and J) and measured lipid levels in the NP tissue. Results revealed higher triglyceride and cholesteryl ester levels in the IDD group than in the control (CTR) group (Fig. 1K and L). Similarly, protein expression of PLIN2 and senescence markers (p21 and p16) was significantly elevated in the IDD group compared to the CTR group (Fig. 1M–O and Fig. S1G, H). Finally, RT-PCR analysis showed increased expression of p16, p21, and p53 in the NP tissue of the IDD group relative to the CTR group (Fig. S1I–K).

3.2. Accumulated lipids promoted NP cell senescence

Palmitic acid (PA), a saturated fatty acid, is commonly used to induce lipid accumulation *in vitro* [31]. In this study, we treated rat NP cells with PA for 24 h and found that PA at 100 μ M and 200 μ M significantly increased triglyceride and cholesteryl ester levels (Fig. 2A and B). Notably, 200 μ M PA treatment significantly enhanced PLIN2 expression (Fig. 2C and D). TEM analysis and BODIPY staining revealed a marked increase in LDs with increasing PA concentration (Fig. 2E and F). Moreover, WB and IF analyses confirmed that 200 μ M PA markedly upregulated the expression of senescence markers p53, p21, and p16 (Fig. 2G–J and Fig. S2 A, B). β -galactosidase staining showed that PA induced senescence in a concentration-dependent manner (Fig. 2K and L). Furthermore, 100 μ M and 200 μ M PA significantly inhibited cell proliferation (Fig. 2M and N), and PA treatment decreased the proportion of cells in the S phase (Fig. 2O).

To further investigate the role of lipid accumulation in NP cell senescence, we inhibited LDs hydrolysis via loss-of-function of adipose triglyceride lipase (ATGL). After 24 h of PA treatment to form LDs, the medium was replaced with lipid-depleted serum (C3840, Vivacell, China). The groupings and experimental procedures are shown in Fig. 2P. WB results showed that knocking down ATGL upregulated the expression of the lipid droplet marker PLIN2 (Fig. 2Q and R). Furthermore, after ATGL knockdown, cellular senescence was exacerbated (Fig. 2S–X).

3.3. Identification of key genes using scRNA-Seq and RNA-Seq combined with machine learning

This study analyzed the single-cell transcriptome of NP tissue samples. Using Seurat, we imported the expression data and filtered cells based on UMI count, gene expression count, and mitochondrial read percentage. Cells deviating more than three median absolute deviations (MAD) from the median were considered outliers, resulting in 9343 cells

for analysis (Fig. S3A–E). The top 10 genes by standard deviation were displayed (Fig. S3F and G). Principal component analysis (PCA) revealed batch effects, which were corrected using Harmony (Fig. S4A and B), with 20 principal components selected based on the ElbowPlot (Fig. S4C). Uniform manifold approximation and projection (UMAP) identified nine subtypes (Fig. S4D), later annotated into eight cell types, including NP cells and several chondrocyte subtypes (Fig. 3A). A bubble plot visualized canonical markers and group proportions (Fig. S4E and F).

Next, we identified 308 lipid metabolism-related genes from the literature [32] and quantified scores using single-sample gene set enrichment analysis (ssGSEA). Results showed that the lipid metabolism score of NP cells was significantly higher in the IDD group than in the CTR group, designating NP cells as a key cell subtype in IDD (Fig. 3B and C). Consequently, NP cells were extracted for differential analysis. Screening criteria were set at $p_{\text{val adj}} < 0.05$, yielding a total of 60 genes (Fig. 3D). Pathway enrichment analysis of these genes, using the Metascape database, indicated enrichment in pathways related to fatty acid metabolism, extracellular matrix, and carboxylic acid metabolic processes (Fig. S4G).

We obtained Series Matrix files for GSE245147 and GSE186542 from the NCBI GEO database. Batch effects were corrected using the SVA algorithm, and PCA plots visualized reduced batch variation post-correction (Fig. S4H and I). To identify key genes among 60 candidates, we applied lasso regression and random forest for feature selection. Lasso regression identified 11 IDD feature genes (Fig. 3E and F), while random forest identified the top 10 (Fig. 3G). The intersection of these two methods yielded four key genes: RDH11, ACTG1, LAMP1, and LGALS1 (Fig. 3H). Single-cell analysis found differential expression of ACTG1, LAMP1, and LGALS1 between the IDD and CTR groups, while RDH11 showed no significant difference (Fig. 3I; Fig. S5A–E). Additionally, GSEA showed ACTG1 enriched in MYC_TARGETS_V1 and OXIDATIVE_PHOSPHORYLATION, LAMP1 in MYOGENESIS, LGALS1 in MYC_TARGETS_V2, and RDH11 in MTORC1_SIGNALING (Fig. S5F–I).

3.4. LAMP1 suppressed lipid accumulation and senescence in NP cells

LAMP1 is a transmembrane glycoprotein located on the lysosomal membrane [33]. Studies suggest that LAMP1 is a key regulatory factor in lipophagy, where its localization and distribution are essential for LD fusion with lysosomes. LAMP1 deficiency or abnormalities can impair LD degradation, resulting in lipid accumulation [34]. To investigate the regulatory role of LAMP1 in lipid metabolism and senescence in NP cells, we first examined LAMP1 expression in mildly and severely degenerated NP tissues using IHC and RT-qPCR assays. Results showed decreased LAMP1 expression in severely degenerated NP tissues (Fig. 4A and B and Fig. S6A). Similarly, in the rat IDD model, LAMP1 expression was also downregulated (Fig. 4C and D).

Next, we transfected NP cells with plasmids to overexpress LAMP1 for 72 h (Fig. S6B and C), followed by PA treatment for 24 h. Lipid assays demonstrated that LAMP1 overexpression inhibited PA-induced increases in triglyceride and cholesteryl ester levels (Fig. 4E and F). Furthermore, WB results indicated that LAMP1 overexpression suppressed PLIN2 protein expression (Fig. 4G and H). In addition, LDs staining revealed that PA significantly increased lipid accumulation in NP cells, but this effect was reversed by LAMP1 overexpression (Fig. 4I). Finally, β -galactosidase staining showed that LAMP1 overexpression reduced NP cell senescence, and WB results further confirmed a reduction in the expression levels of senescence markers following LAMP1 overexpression (Fig. 4J and K).

3.5. Sulforaphane promoted LAMP1 expression and lipophagy

SFN, a natural isothiocyanate compound (Fig. 5A), is primarily found in cruciferous vegetables such as broccoli. SFN plays multiple roles in regulating lipid metabolism, including inhibiting lipid synthesis and

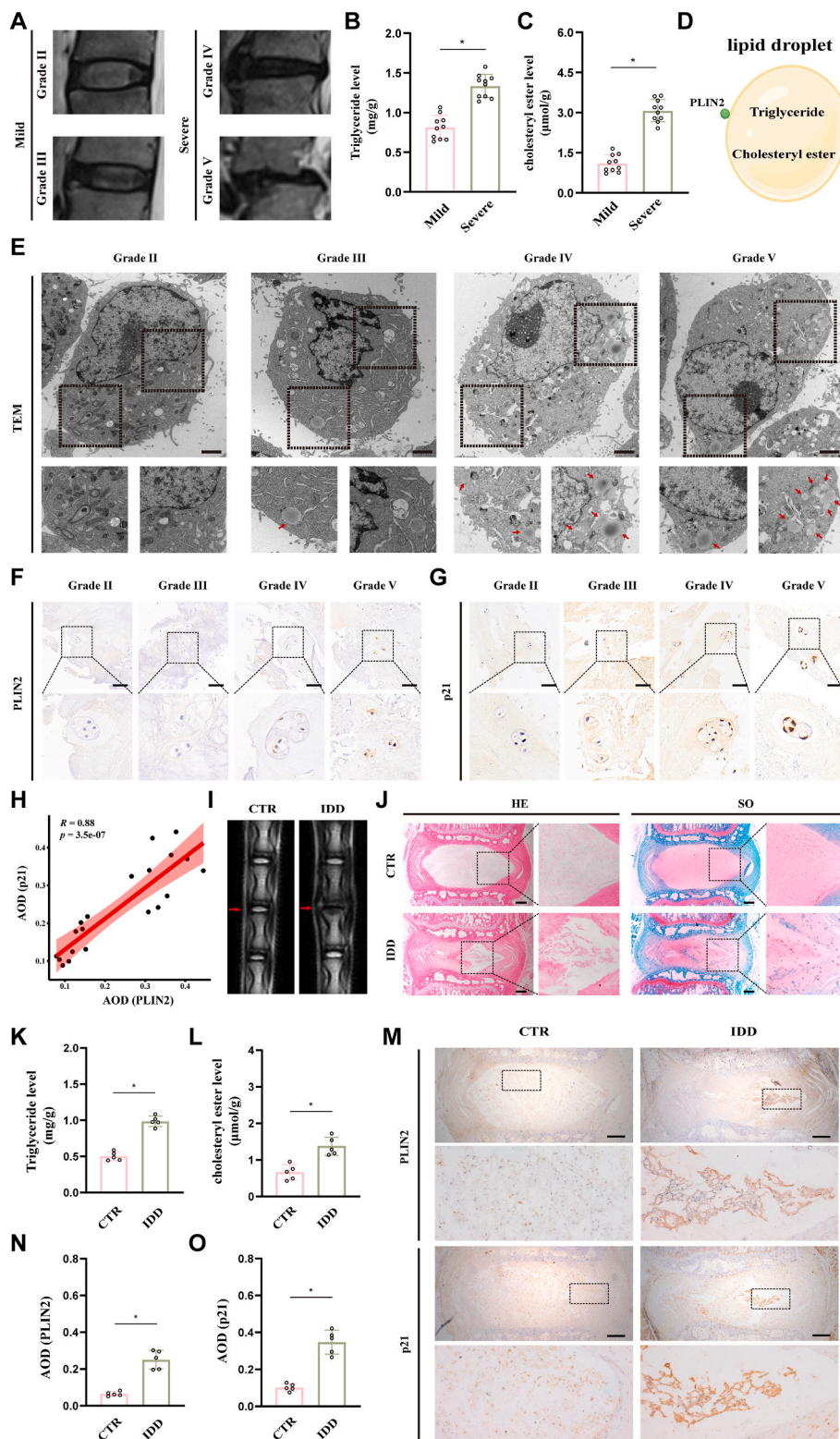


Fig. 1. Lipid accumulation in degenerated NP tissue and its association with senescence. (A) Lumbar spine MRI images showing varying degrees of IDD. (B) Triglyceride content in human NP tissue. (C) Cholesterol ester content in human NP tissue. (D) Schematic diagram of LD structure. (E) LDs in human NP cells observed by TEM, the red arrow indicates the LDs, scale bar = 5 μM. (F) IHC staining of PLIN2 in human NP tissue, scale bar = 100 μM. (G) IHC staining of p21 in human NP tissue, scale bar = 100 μM. (H) Correlation analysis between PLIN2 and p21 expression levels. (I) MRI of rat caudal vertebrae. (J) HE and SO staining of rat caudal intervertebral discs, scale bar = 500 μM. (K) Triglyceride content in rat NP tissue. (L) Cholesterol ester content in rat NP tissue. (M) IHC staining of PLIN2 and p21 in rat NP tissue, scale bar = 500 μM. (N and O) average optical density (AOD) analysis in (M). Data are represented as mean ± SD, **p* < 0.05.

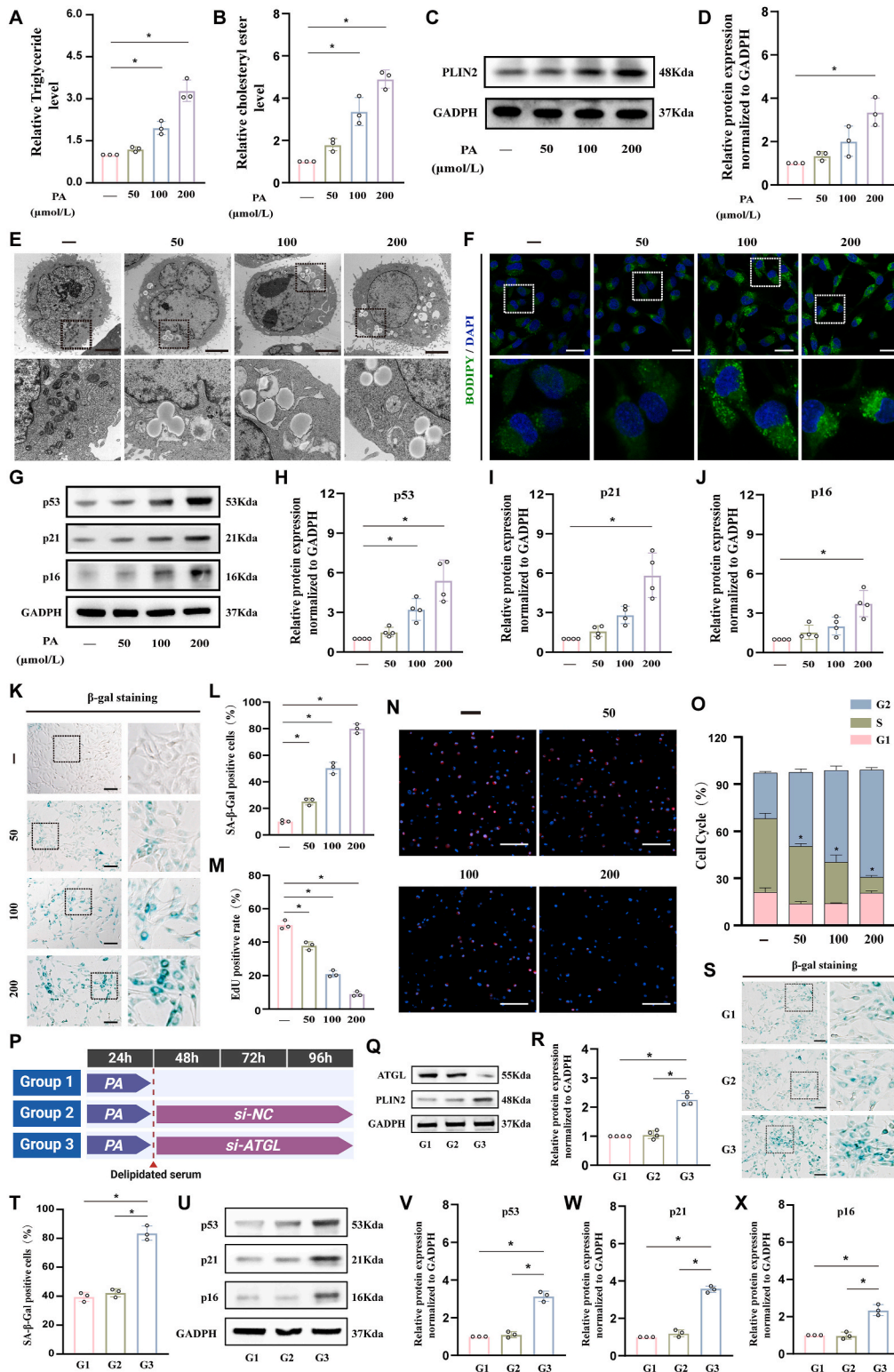
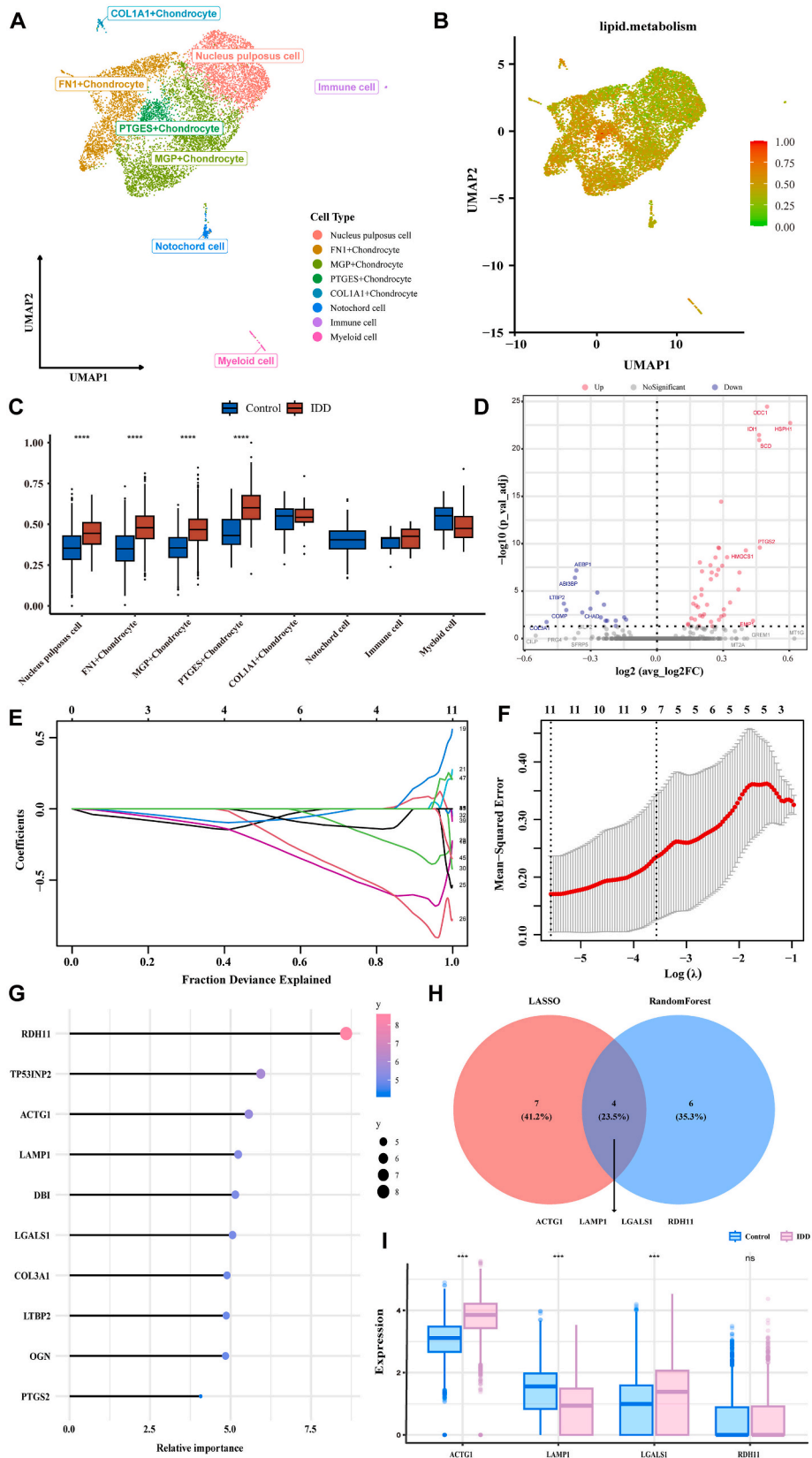


Fig. 2. Accumulated lipids promoted NP cell senescence. (A) Triglyceride content in rat NP cells after PA treatment. (B) Cholesterol ester content in rat NP cells after PA treatment. (C and D) Expression of PLIN2 in rat NP cells after PA treatment, detected by WB. (E) LDs in rat NP cells after PA treatment, observed by TEM, scale bar = 5 μM. (F) LDs in rat NP cells after PA treatment, observed with Biodipy staining, scale bar = 50 μM. (G–J) Expression of senescence markers (p53, p21, and p16) in rat NP cells after PA treatment, detected by Western blot. (K and L) Senescence of rat NP cells after PA treatment, detected by β-galactosidase staining, scale bar = 100 μM. (M and N) Proliferation of rat NP cells after PA treatment, detected by EDU staining, scale bar = 500 μM. (O) Cell cycle distribution of rat NP cells after PA treatment, analyzed by flow cytometry. (P) Experimental setup for LD hydrolysis inhibition via ATGL knockdown after PA treatment in NP cells. (Q and R) Expression of senescence markers in rat NP cells after PA or siATGL treatment. (S and T) Senescence of rat NP cells, detected by β-galactosidase staining, scale bar = 100 μM. (U–X) Expression of senescence markers in rat NP cells after PA treatment and siLAMP1 transfection. Data are represented as mean ± SD, **p* < 0.05.



(caption on next page)

Fig. 3. Identification of key genes using scRNA-Seq and RNA-Seq combined with machine learning. (A) UMAP plot showing the clustering of single cells from degenerated and normal NP tissues. (B and C) Lipid metabolism analysis, with visualizations representing differential genes and pathways involved in lipid metabolism. (D) The volcano plot shows the genes with significantly upregulated and downregulated lipid scores between degenerated and normal NP tissues. (E) Lasso regression plot showing the selection of key genes that differentiate between degenerated and normal NP tissues. (F) Cross-validation plot for the Lasso model, displaying optimal lambda values for feature selection, which minimizes prediction error in distinguishing tissue states. (G) RF importance plot highlighting key genes identified by RF analysis. (H) Venn diagram summarizing the overlap of selected genes identified by Lasso and RF models, pinpointing common critical genes. (I) Expression profile of identified key genes, comparing expression levels between degenerated and normal NP tissues to highlight differential expression patterns.

promoting fatty acid oxidation [35,36]. Additionally, studies have shown that SFN can act as an activator of LAMP1, thereby upregulating the expression of LAMP1 [37,38]. To investigate whether SFN inhibits lipid accumulation and senescence through LAMP1, we first assessed the effect of SFN on NP cell viability using a CCK8 assay. Results indicated that 5 μ M SFN had no adverse effect on NP cells over 24–72 h (Fig. S6D–F). Molecular docking analysis showed that SFN formed hydrogen bonds with LAMP1, with a binding energy of -2.9 kcal/mol, suggesting relatively weak binding stability (Fig. S6G and H).

Next, we treated NP cells with both SFN and PA for 24 h to evaluate SFN's regulatory effects on LAMP1 and autophagy. WB results showed that SFN significantly increased LAMP1 expression and the LC3 II/I ratio, while markedly reducing p62 expression (Fig. 5B and C). IF results similarly demonstrated that SFN enhanced both LAMP1 expression and autophagy (Fig. 5D–G). CO-IP results indicated that SFN promoted the interaction between LAMP1 and LC3II (Fig. 5H), suggesting that SFN facilitates the fusion of lysosomes and autophagosomes. TEM revealed numerous autolysosomes surrounding LDs in SFN-treated NP cells (Fig. 5I), indicating that SFN promotes lipophagy. Supporting these findings, IF demonstrated that SFN treatment increased the colocalization of LAMP1 with LDs, as well as LC3 with LDs (Fig. 5J–M). In addition, SFN inhibited the elevated ROS levels induced by PA (Fig. S6I and J), with a significant reduction in lipid peroxidation levels and MDA content following SFN treatment (Fig. S6K–M).

3.6. Activation of LAMP1-mediated lipophagy by sulforaphane inhibited senescence

To further investigate whether SFN inhibited lipid accumulation and senescence via LAMP1, we first transfected rat NP cells with siRNA for 72 h to knock down LAMP1 expression (Fig. S7A and B), followed by treatment with PA and SFN for 24 h. Results showed that SFN treatment significantly reduced triglyceride and cholesteryl ester levels in NP cells; however, this effect was reversed following LAMP1 knockdown (Fig. 6A and B). WB analysis indicated that the SFN-induced downregulation of PLIN2 expression was restored upon LAMP1 knockdown (Fig. 6C and D). BODIPY staining further demonstrated that the reduction in lipid accumulation by SFN was reversed after LAMP1 knockdown (Fig. 6E). Additionally, the SFN-induced decrease in senescence and increase in cell proliferation were also reversed by LAMP1 knockdown (Fig. 6F). And SFN treatment significantly increased the proportion of S-phase cells, but this effect was diminished following LAMP1 knockdown (Fig. 6G and H). The expression levels of p53, p21, and p16 were significantly reduced with SFN treatment but were markedly upregulated upon LAMP1 knockdown (Fig. 6I–K).

3.7. Sulforaphane attenuated lipid accumulation and senescence in a rat IDD model

To validate the role of SFN in IDD in vivo, we administered an SFN injection following needle puncture in a rat disc model (Fig. 7A). MRI revealed that the signal intensity of NP tissue was significantly reduced in the IDD group compared to the sham group, whereas SFN injection markedly restored signal intensity (Fig. 7B and C). X-ray results showed that the disc height index (DHI) was significantly reduced in the IDD group compared to the sham group, but increased following SFN injection (Fig. 7B–D). HE and SO staining indicated that, compared to the sham group, the NP area in the IDD group was significantly reduced,

with disordered NP cell arrangement, disrupted AF structure, and decreased disc height. After SFN injection, the NP area significantly increased, NP cell distribution was more uniform, and AF structure was largely restored (Fig. 7E and F).

We then evaluated the effect of SFN on lipid metabolism and senescence in vivo. Results showed that triglyceride and cholesteryl ester levels were elevated in the IDD group but were partially reversed by SFN treatment (Fig. S7C and D). Additionally, IHC results showed that LAMP1 expression was downregulated in the IDD group but upregulated following SFN treatment, with opposing trends observed for PLIN2, p16, and p21 expression (Fig. 7G–J and Fig. S7E and F). Meanwhile, the IF results showed that in the IDD group, LAMP1 expression decreased, while PLIN2 and p21 levels increased. However, in the SFN-treated group, LAMP1 expression was restored, and PLIN2 and p21 levels decreased (Fig. 7K).

4. Discussion

IDD is closely associated with several metabolic diseases, including diabetes, obesity, and dyslipidemia [39,40]. Dyslipidemia, a significant metabolic risk factor, can exacerbate disc degeneration by disrupting the disc's microcirculation and metabolic environment [41,42]. Multiple clinical studies have shown that elevated serum cholesterol and triglyceride levels are important independent risk factors for IDD [14,15,43]. However, the intervertebral disc is the largest avascular tissue in the human body; it primarily relies on nutrient diffusion through the endplate rather than a direct blood supply [44]. Furthermore, endplate calcification during degeneration restricts diffusion, suggesting that the reduced blood supply associated with dyslipidemia is not the primary driver of IDD [45]. This highlights the need to explore alternative underlying mechanisms.

Recent studies suggest that IDD may induce lipid metabolism abnormalities in NP cells. Using nuclear magnetic resonance (NMR) spectroscopy, Toczyłowska et al. [46] identified significant changes in lipid types and content in degenerated NP tissues, including abnormal accumulation of monoglycerides and triglycerides. Additionally, metabolomics analysis revealed elevated triglyceride levels in severely degenerated NP tissues [18]. However, other studies did not detect significant lipid metabolism abnormalities in degenerated NP tissues [22]. Given these discrepancies, we employed multiple methods—including LD staining, triglyceride and cholesteryl ester quantification, and analysis of LD-associated protein PLIN2 expression. Our results confirmed lipid accumulation in degenerated NP tissues and demonstrated that this lipid accumulation was closely associated with NP cell senescence. Further investigation revealed that knockdown of ATGL (a key lipase for LDs hydrolysis) expression in PA-treated NP cells significantly aggravated NP cell senescence. In addition, Chen et al. [18] induced lipid accumulation in NP cells using PA and found that the expression levels of senescence markers were also upregulated, further supporting the close relationship between lipid accumulation and NP cell senescence.

Dysregulated lipid metabolism plays a significant role in IDD, and targeting lipid metabolism has emerged as a promising strategy to delay degeneration [47]. Studies have shown that natural hydrogel complexes can slow IDD progression by modulating fatty acid metabolism [48]. Nimbolide, a natural triterpenoid compound, alleviates NP cell damage caused by cholesterol accumulation by promoting cholesterol efflux and suppressing inflammatory signaling pathways [49]. Additionally, the

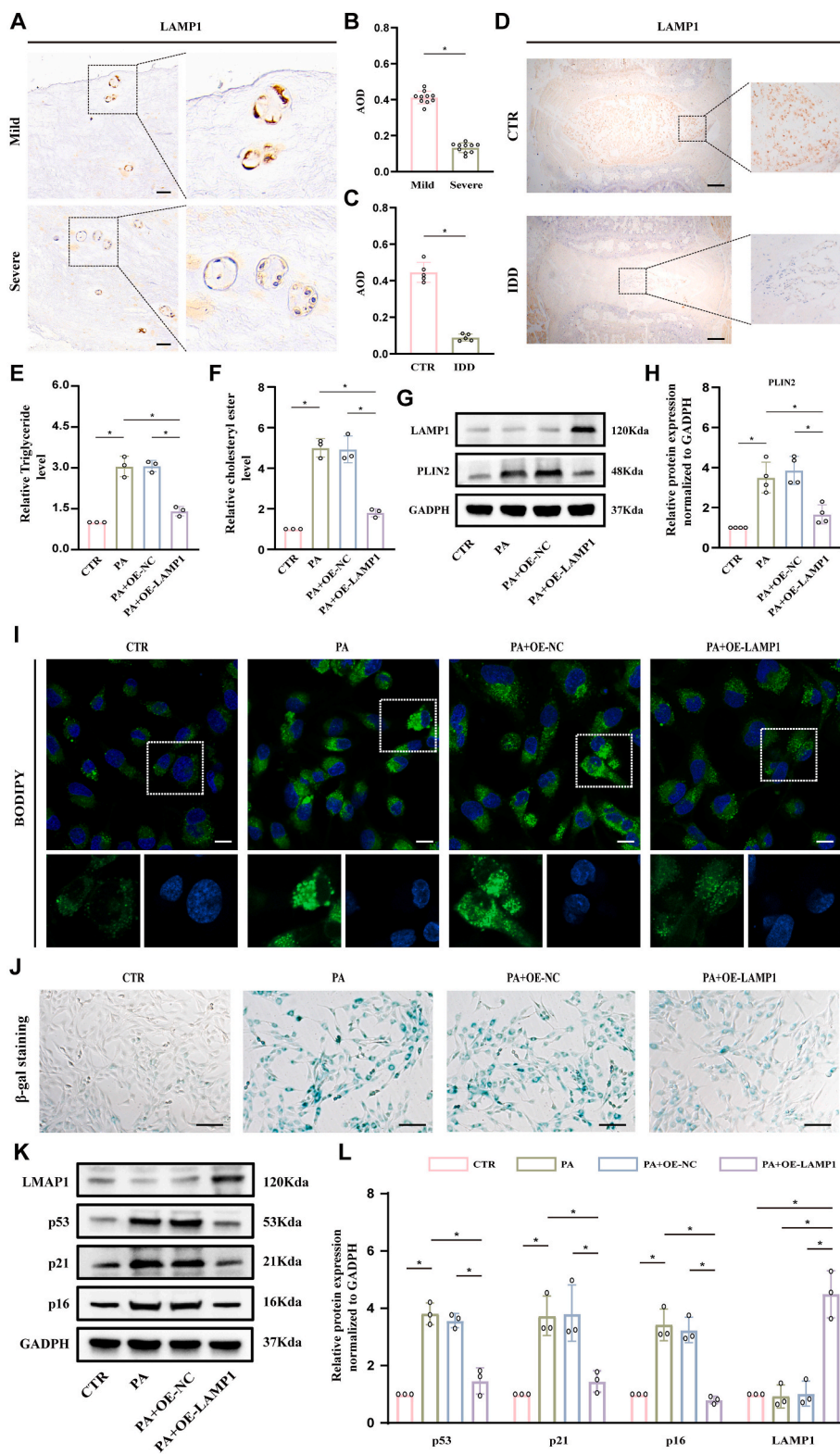


Fig. 4. LAMP1 suppressed lipid accumulation and senescence in NP cells. (A and B) Immunohistochemical detection of LAMP1 expression in mildly and severely degenerated NP tissues, scale bar = 100 μm. (C and D) LAMP1 expression in normal and degenerated rat NP tissues, scale bar = 500 μm. (E) Triglyceride content in rat NP cells after PA treatment and LAMP1 overexpression. (F) Cholesterol ester content in rat NP cells after PA treatment and LAMP1 overexpression. (G and H) Expression of LAMP1 and PLIN2 in rat NP cells after PA treatment and LAMP1 overexpression, detected by Western blot. (I) LDs in rat NP cells after PA treatment and LAMP1 overexpression, observed with Biodipy staining, scale bar = 50 μm. (J) Senescence of rat NP cells after PA treatment and LAMP1 overexpression, detected by β-galactosidase staining, scale bar = 100 μm. (K and L) Expression of senescence markers (p53, p21, and p16) in rat NP cells after PA treatment and LAMP1 overexpression, detected by Western blot. Data are represented as mean ± SD, **p* < 0.05.

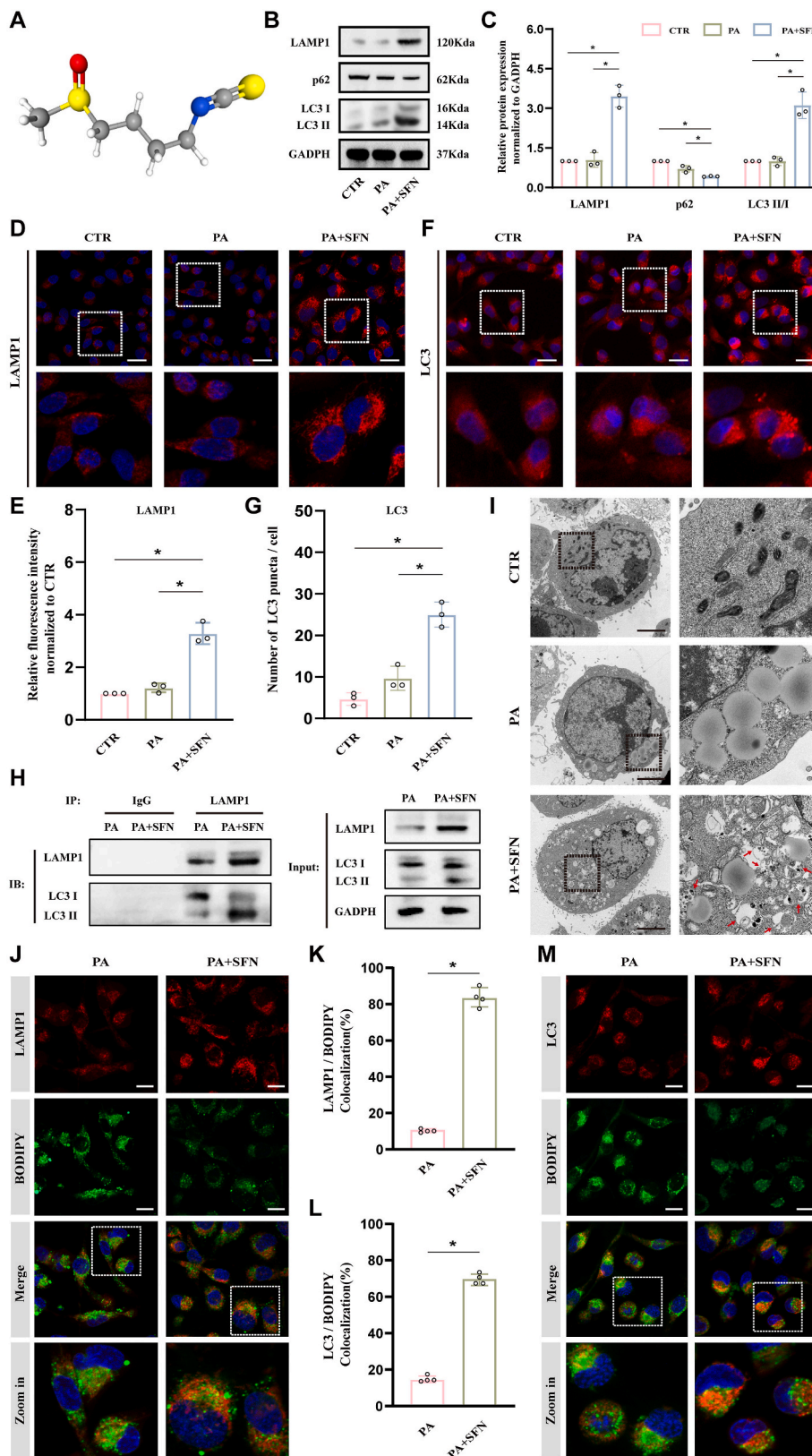


Fig. 5. SFN promoted LAMP1 expression and lipophagy. (A) Chemical structure of SFN. (B and C) Expression of LAMP1 and autophagy markers (P62 and LC3) in rat NP cells after PA and SFN treatment, detected by WB. (D and E) LAMP1 expression in rat NP cells after PA and SFN treatment, observed by immunofluorescence, scale bar = 50 μ m. (F and G) LC3 expression in rat NP cells after PA and SFN treatment, observed by fluorescence microscopy, scale bar = 50 μ m. (H) Interaction between LAMP1 and LC3 in rat NP cells after PA and SFN treatment, detected by Co-IP. (I) LDs in rat NP cells after PA and SFN treatment, observed by TEM, the red arrow indicates the autolysosomes, scale bar = 5 μ m. (J and K) Co-localization of LAMP1 and LDs in rat NP cells after PA and SFN treatment, observed by fluorescence microscopy, scale bar = 30 μ m. (L and M) Co-localization of LC3 and LDs in rat NP cells after PA and SFN treatment, observed by fluorescence microscopy, scale bar = 30 μ m. Data are represented as mean \pm SD, * p < 0.05.

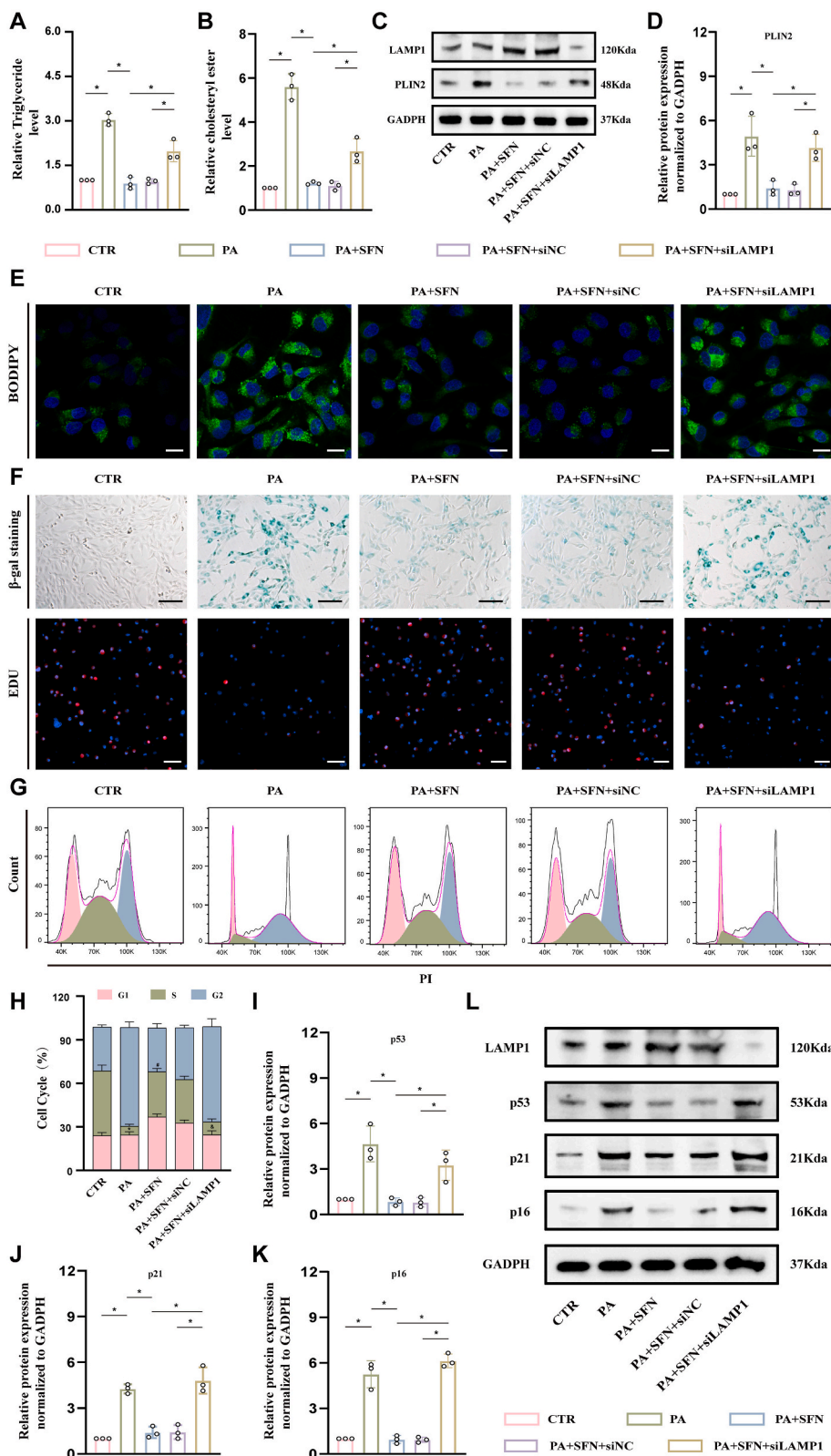


Fig. 6. SFN delayed senescence in NP cells through LAMP1-mediated lipophagy. (A) Triglyceride content in rat NP cells after PA, SFN treatment, and siRNA-LAMP1 transfection. (B) Cholesterol ester content in rat NP cells after PA, SFN treatment, and siRNA-LAMP1 transfection. (C and D) Expression of LAMP1 and PLIN2 in rat NP cells after PA, SFN treatment, and siRNA-LAMP1 transfection, detected by Western blot. (E) LDs in rat NP cells after PA, SFN treatment, and siRNA-LAMP1 transfection, observed with Biodipy staining, scale bar = 50 μm. (F) Senescence and proliferation of rat NP cells after PA, SFN treatment, and siRNA-LAMP1 transfection, scale bar = 100 μm (white light images), scale bar = 500 μm (IF images). (G and H) Cell cycle distribution of rat NP cells after transfection with LAMP1 siRNA, analyzed by flow cytometry, *p < 0.05 compared with CTR group; #p < 0.05 compared with PA group; &p < 0.05 compared with PA + SFN group. (I-L) Expression of senescence markers in rat NP cells after PA, SFN treatment, and siRNA-LAMP1 transfection, detected by Western blot. Data are represented as mean ± SD, *p < 0.05.

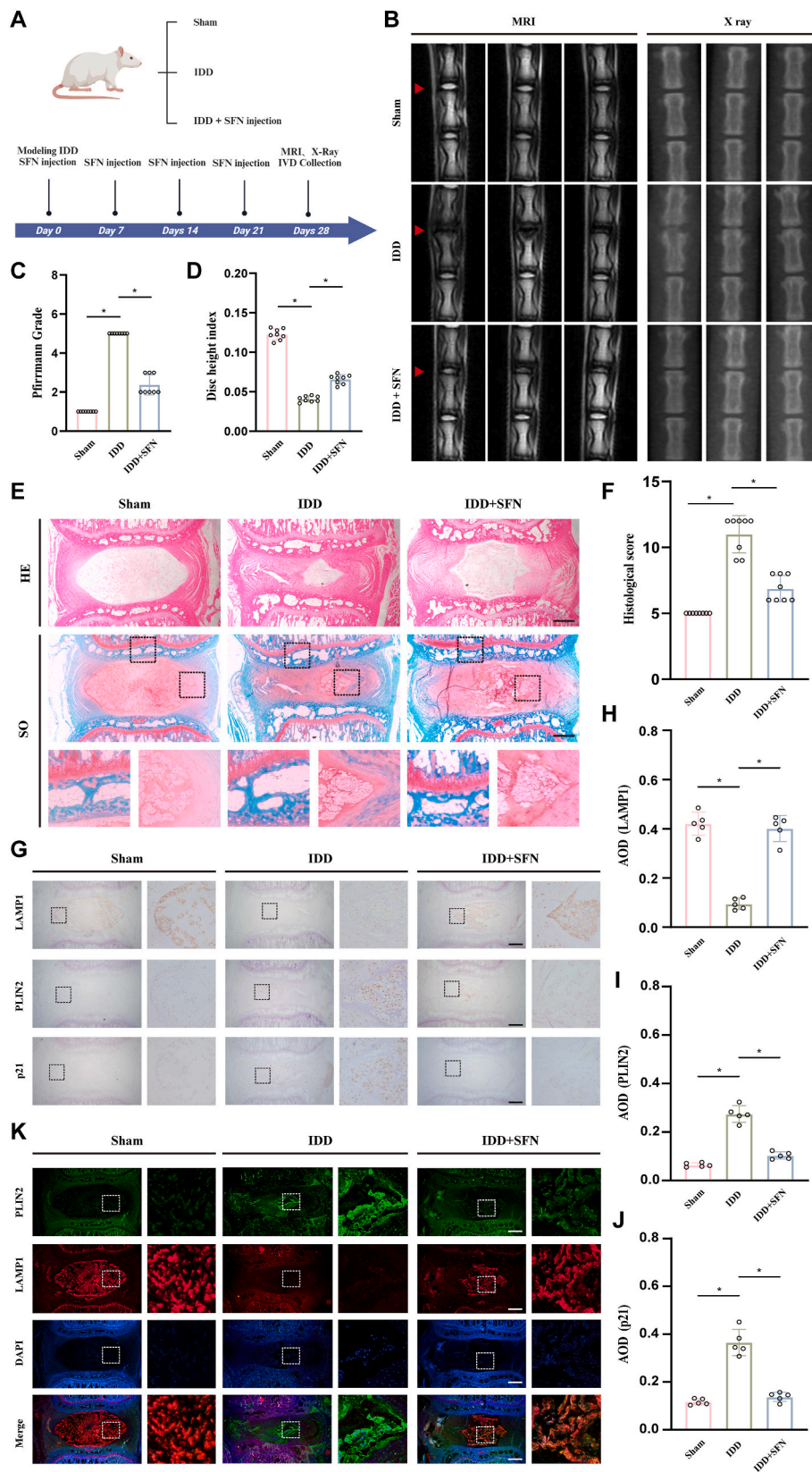


Fig. 7. SFN attenuated lipid accumulation and senescence in a rat IDD model. (A) Schematic diagram of the experimental protocol in SD rats. (B) MRI and X-ray images of rat caudal vertebrae. (C) Assessment of rat IDD using the Pfirrmann grading system. (D) Evaluation of changes in intervertebral disc height (DHI) in rats. (E and F) Evaluation and scoring of rat IDD using HE staining and Safranin O-Fast Green staining, scale bar = 500 μm. (G–J) Immunohistochemical detection of LAMP1, PLIN2, and p21 expression in rat NP tissue, scale bar = 500 μm. (K) Immunofluorescence detection of LAMP1 and PLIN2 expression in rat NP tissue, scale bar = 500 μm. Data are represented as mean ± SD, **p* < 0.05.

miR-155/ROR α pathway has been identified as a target for mitigating cholesterol-induced matrix degradation and NP cell death [50]. In this study, we discovered that SFN, a natural isothiocyanate compound, effectively promoted lipid clearance within NP cells. Mechanistic investigations revealed that SFN upregulated the expression of LAMP1, thereby activating lipophagy pathways. This process significantly reduced intracellular lipid accumulation and inhibited cellular senescence. *In vivo* experiments further confirmed that SFN mitigated disc degeneration in animal models, highlighting its potential in regulating lipid metabolism to delay IDD progression.

Lipophagy, the process by which cells degrade LDs, is essential for maintaining intracellular lipid homeostasis [51]. LAMP1 is integral to lipophagy, facilitating the fusion of autophagosomes with lysosomes—a crucial step in LD degradation [52–54]. In our study, we found lipid accumulation and low expression of LAMP1 in degenerated nucleus pulposus tissues. Furthermore, overexpression of LAMP1 significantly reduced lipid accumulation and senescence in NP cells. However, another study has shown that upregulation of LAMP1 in prostate cancer cells promotes cellular senescence [34]. This contradictory finding may be due to the specific functions and microenvironmental differences across cell types. In cancer cells, lysosomal functions may be reprogrammed, with increased LAMP1 expression promoting lysosome-mediated cell death pathways. Therefore, the role of LAMP1 in different cell types requires further analysis within the context of specific cellular environments and disease states.

Sulforaphane is a natural compound derived from cruciferous vegetables such as broccoli, known for its potent antioxidant, anti-inflammatory, and anticancer properties [55]. Studies have shown that SFN enhances LAMP1 expression by activating the Nrf2 signaling pathway. Specifically, SFN relieves the inhibition of Nrf2 by Keap1, allowing Nrf2 to translocate to the nucleus, where it binds to the promoter of LAMP1 [38,56]. Moreover, SFN plays a crucial role in regulating lipid metabolism. For instance, SFN was shown to promote lipophagy and lysosome biogenesis by activating the TFEB/NFE2L2 pathway, thereby reducing damaged lipid accumulation and improving oxidative stress [37]. Additionally, in studies on lipid accumulation induced by high-fat diets, SFN improved hepatocyte lipid homeostasis by accelerating LD degradation via the Nrf2 pathway [36]. In our study, we found that SFN not only promoted the expression of LAMP1 and LC3II but also enhanced their interaction, suggesting that SFN effectively stimulates lipophagy. When LAMP1 expression was knocked down, the SFN-induced reduction in lipid accumulation and inhibition of senescence were reversed, confirming the essential role of LAMP1 in SFN-induced lipophagy. Additionally, previous studies have shown that SFN reduces oxidative stress and apoptosis in NP cells, indicating the protective effect of SFN on NP cells [57].

In conclusion, this study provides the first comprehensive analysis of the regulatory mechanisms of LAMP1-mediated lipophagy in controlling lipid accumulation and senescence in NP cells. Our findings reveal the potential therapeutic role of sulforaphane in delaying the progression of IDD, offering new targets and strategies for treating this degenerative condition.

Author contributions

Houqing Long, Guozhi Xiao and Songlin Peng conceived and designed the study. Tianyu Qin, Ming Shi and Yongheng Xie performed the experiments. Tianyu Qin, Naibo Feng and Chungeng Liu analyzed the results. Tianyu Qin, Ke Chen and Yining Chen were responsible for data collection. Wanli Zheng and Mingxi Zhu contributed to the literature search and specimen collection. Guozhi Xiao and Tianyu Qin wrote and edited the manuscript.

Data availability

The data that support the findings of this study are available from the

corresponding author upon reasonable request.

Funding

This study was funded by the National Natural Science Foundation of China (No.82302031), the Guangdong Basic and Applied Basic Research Fund Shenzhen Joint Fund of China (2022A151511197), the Introduction of Talent Research Initiation Fund of Shenzhen People's Hospital (20200322-1, Houqing Long).

Declaration of competing interest

The authors declare that they have no known competing financial interests or personal relationships that could have appeared to influence the work reported in this paper.

Appendix A. Supplementary data

Supplementary data to this article can be found online at <https://doi.org/10.1016/j.jot.2025.05.010>.

References

- [1] Chen S, Chen M, Wu X, Lin S, Tao C, Cao H, et al. Global, regional and national burden of low back pain 1990–2019: a systematic analysis of the Global Burden of Disease study 2019. *J Orthop Translat* 2021;32:49–58.
- [2] Dieleman JL, Cao J, Chapin A, Chen C, Li Z, Liu A, et al. US health care spending by payer and health condition, 1996–2016. *JAMA* 2020;323(9):863–84.
- [3] Traeger AC, Underwood M, Ivers R, Buchbinder R. Low back pain in people aged 60 years and over. *BMJ* 2022;376:e066928.
- [4] Francisco V, Pino J, González-Gay MÁ, Lago F, Karppinen J, Tervonen O, et al. A new immunometabolic perspective of intervertebral disc degeneration. *Nat Rev Rheumatol* 2022;18(1):47–60.
- [5] Wang Y, Cheng H, Wang T, Zhang K, Zhang Y, Kang X. Oxidative stress in intervertebral disc degeneration: molecular mechanisms, pathogenesis and treatment. *Cell Prolif* 2023;56(9):e13448.
- [6] Song Y, Liang H, Li G, Ma L, Zhu D, Zhang W, et al. The NLRX1-SLC39A7 complex orchestrates mitochondrial dynamics and mitophagy to rejuvenate intervertebral disc by modulating mitochondrial Zn(2+) trafficking. *Autophagy* 2024;20(4):809–29.
- [7] Chen M, Li F, Qu M, Jin X, He T, He S, et al. Pip5k1 γ promotes anabolism of nucleus pulposus cells and intervertebral disc homeostasis by activating CaMKII-Ampk pathway in aged mice. *Aging Cell* 2024;23(9):e14237.
- [8] Tu J, Li W, Yang S, Yang P, Yan Q, Wang S, et al. Single-cell transcriptome profiling reveals multicellular ecosystem of nucleus pulposus during degeneration progression. *Adv Sci (Weinh)* 2022;9(3):e2103631.
- [9] Yoon H, Shaw JL, Haigis MC, Greka A. Lipid metabolism in sickness and in health: emerging regulators of lipotoxicity. *Mol Cell* 2021;81(18):3708–30.
- [10] Park S, Baek IJ, Ryu JH, Chun CH, Jin EJ. PPAR α -ACOT12 axis is responsible for maintaining cartilage homeostasis through modulating de novo lipogenesis. *Nat Commun* 2022;13(1):3.
- [11] McGee-Lawrence ME, Carpio LR, Schulze RJ, Pierce JL, McNiven MA, Farr JN, et al. Hdac3 deficiency increases marrow adiposity and induces lipid storage and glucocorticoid metabolism in osteochondroprogenitor cells. *J Bone Miner Res* 2016;31(1):116–28.
- [12] Guymer RH, Campbell TG. Age-related macular degeneration. *Lancet* 2023;401(10386):1459–72.
- [13] Haney MS, Pálovics R, Munson CN, Long C, Johansson PK, Yip O, et al. APOE4/4 is linked to damaging lipid droplets in Alzheimer's disease microglia. *Nature* 2024;13(1):38.
- [14] Yuan L, Huang Z, Han W, Chang R, Sun B, Zhu M, et al. The impact of dyslipidemia on lumbar intervertebral disc degeneration and vertebral endplate modic changes: a cross-sectional study of 1035 citizens in China. *BMC Public Health* 2023;23(1):1302.
- [15] Zhang X, Chen J, Huang B, Wang J, Shan Z, Liu J, et al. Obesity mediates apoptosis and extracellular matrix metabolic imbalances via MAPK pathway activation in intervertebral disk degeneration. *Front Physiol* 2019;10:1284.
- [16] Bing T, Shanlin X, Jisheng W, Jie H, Ruichao C, Zhiwei Z, et al. Dysregulated lipid metabolism and intervertebral disc degeneration: the important role of ox-LDL/LOX-1 in endplate chondrocyte senescence and calcification. *Mol Med* 2024;30(1):117.
- [17] Yan J, Li S, Zhang Y, Deng Z, Wu J, Huang Z, et al. Cholesterol induces pyroptosis and matrix degradation via mSREBP1-driven endoplasmic reticulum stress in intervertebral disc degeneration. *Front Cell Dev Biol* 2021;9:803132.
- [18] Chen X, Chen K, Hu J, Dong Y, Zheng M, Jiang J, et al. Palmitic acid induces lipid droplet accumulation and senescence in nucleus pulposus cells via ER-stress pathway. *Commun Biol* 2024;7(1):539.

- [19] Keser N, Celikoglu E, Is M, İlgezdi ZD, Sunar B, Aydın YS, et al. Is there a relationship between blood lipids and lumbar disc herniation in young Turkish adults? *Arch Med Sci Atheroscler Dis* 2017;2(1):e24–8.
- [20] Kerr GJ, To B, White I, Millicamps M, Beier F, Grol MW, et al. Diet-induced obesity leads to behavioral indicators of pain preceding structural joint damage in wild-type mice. *Arthritis Res Ther* 2021;23(1):93.
- [21] D'Erminio DN, Krishnamoorthy D, Lai A, Hoy RC, Natelson DM, Poeran J, et al. High fat diet causes inferior vertebral structure and function without disc degeneration in RAGE-KO mice. *J Orthop Res* 2022;40(7):1672–86.
- [22] Francisco V, Ait Eldjoudi D, González-Rodríguez M, Ruiz-Fernández C, Cordero-Barreal A, Marques P, et al. Metabolomic signature and molecular profile of normal and degenerated human intervertebral disc cells. *Spine J* 2023;23(10):1549–62.
- [23] de Magalhães JP. Cellular senescence in normal physiology. *Science* 2024;384(6702):1300–1.
- [24] Nguyen D, Samson SL, Reddy VT, Gonzalez EV, Sekhar RV, et al. Impaired mitochondrial fatty acid oxidation and insulin resistance in aging: novel protective role of glutathione. *Aging Cell* 2013;12(3):415–25.
- [25] Xu F, Hua C, Tautenhahn HM, Dirsch O, Dahmen U. The role of autophagy for the regeneration of the aging liver. *Int J Mol Sci* 2020;21(10):3606.
- [26] Sharma A, Smith HJ, Yao P, Mair WB. Causal roles of mitochondrial dynamics in longevity and healthy aging. *EMBO Rep* 2019;20(12):e48395.
- [27] Kim YM, Shin HT, Seo YH, Byun HO, Yoon SH, Lee IK, et al. Sterol regulatory element-binding protein (SREBP)-1-mediated lipogenesis is involved in cell senescence. *J Biol Chem* 2010;285(38):29069–77.
- [28] Chung KW. Advances in understanding of the role of lipid metabolism in aging. *Cells* 2021;10(4):880.
- [29] Liu Y, Dou Y, Sun X, Yang Q. Mechanisms and therapeutic strategies for senescence-associated secretory phenotype in the intervertebral disc degeneration microenvironment. *J Orthop Translat* 2024;45:56–65.
- [30] Li G, Ma L, He S, Luo R, Wang B, Zhang W, et al. WTAP-mediated m(6)A modification of lncRNA NORAD promotes intervertebral disc degeneration. *Nat Commun* 2022;13(1):1469.
- [31] Lu J, Meng Z, Cheng B, Liu M, Tao S, Guan S. Apigenin reduces the excessive accumulation of lipids induced by palmitic acid via the AMPK signaling pathway in HepG2 cells. *Exp Ther Med* 2019;18(4):2965–71.
- [32] Lin H, Fu L, Li P, Zhu J, Xu Q, Wang Y, et al. Fatty acids metabolism affects the therapeutic effect of anti-PD-1/PD-L1 in tumor immune microenvironment in clear cell renal cell carcinoma. *J Transl Med* 2023;21(1):343.
- [33] Chaudhry N, Sica M, Surabhi S, Hernandez DS, Mesquita A, Selimovic A, et al. Lamp1 mediates lipid transport, but is dispensable for autophagy in *Drosophila*. *Autophagy* 2022;18(10):2443–58.
- [34] Panda PK, Patra S, Naik PP, Prahara PP, Mukhopadhyay S, Meher BR, et al. Deacetylation of LAMP1 drives lipophagy-dependent generation of free fatty acids by Abrus agglutinin to promote senescence in prostate cancer. *J Cell Physiol* 2020;235(3):2776–91.
- [35] Men X, Han X, Lee SJ, Oh G, Park KT, Han JK, et al. Anti-obesogenic effects of sulforaphane-rich broccoli (*Brassica oleracea* var. *italica*) sprouts and myrosinase-rich mustard (*Sinapis alba* L.) seeds in vitro and in vivo. *Nutrients* 2022;14(18):3814.
- [36] Lei P, Hu Y, Gao P, Ding Q, Yan J, Zhao J, et al. Sulforaphane ameliorates hepatic lipid metabolism via modulating lipophagy in vivo and in vitro. *J Agric Food Chem* 2022;70(48):15126–33.
- [37] Li D, Shao R, Wang N, Zhou N, Du K, Shi J, et al. Sulforaphane Activates a lysosome-dependent transcriptional program to mitigate oxidative stress. *Autophagy* 2021;17(4):872–87.
- [38] Qiu S, Liang Z, Wu Q, Wang M, Yang M, Chen C, et al. Hepatic lipid accumulation induced by a high-fat diet is regulated by Nrf2 through multiple pathways. *FASEB J* 2022;36(5):e22280.
- [39] Song C, Hu P, Peng R, Li F, Fang Z, Xu Y. Bioenergetic dysfunction in the pathogenesis of intervertebral disc degeneration. *Pharmacol Res* 2024;202:107119.
- [40] Kodama J, Wilkinson KJ, Otsuru S. Nutrient metabolism of the nucleus pulposus: a literature review. *N Am Spine Soc J* 2023;13:100191.
- [41] Cai YT, Zhong XX, Mo L, Huang RZ, Lin Q, Liu CJ, et al. Evaluating the causal effect of atherosclerosis on the risk of intervertebral disc degeneration. *JOR Spine* 2024;7(1):e1319.
- [42] Zhang Y, Si M, Li C, Liu Y, Han Y, Nie L, et al. Effect of hyperlipidaemia to accelerate intervertebral disc degeneration in the injured rat caudal disc model. *J Orthop Sci* 2019;24(1):42–9.
- [43] Huang Z, Chen J, Su Y, Guo M, Chen Y, Zhu Y, et al. Impact of dyslipidemia on the severity of symptomatic lumbar spine degeneration: a retrospective clinical study. *Front Nutr* 2022;9:1033375.
- [44] Fournier DE, Kiser PK, Shoemaker JK, Battié MC, Séguin CA. Vascularization of the human intervertebral disc: a scoping review. *JOR Spine* 2020;3(4):e1123.
- [45] Ashinsky BG, Bonnevie ED, Mandalapu SA, Pickup S, Wang C, Han L, et al. Intervertebral disc degeneration is associated with aberrant endplate remodeling and reduced small molecule transport. *J Bone Miner Res* 2020;35(8):1572–81.
- [46] Toczylowska B, Woznica M, Zieminska E, Krolicki L. Metabolic biomarkers differentiate a surgical intervertebral disc from a nonsurgical intervertebral disc. *Int J Mol Sci* 2023;24(13):10572.
- [47] Yi J, Zhou Q, Huang J, Niu S, Ji G, Zheng T. Lipid metabolism disorder promotes the development of intervertebral disc degeneration. *Biomed Pharmacother* 2023;166:115401.
- [48] Wang D, Zhang L, He D, Zhang Y, Zhao L, Miao Z, et al. A natural hydrogel complex improves intervertebral disc degeneration by correcting fatty acid metabolism and inhibiting nucleus pulposus cell pyroptosis. *Mater Today Bio* 2024;26:101081.
- [49] Teng Y, Huang Y, Yu H, Wu C, Yan Q, Wang Y, et al. Nimbolide targeting SIRT1 mitigates intervertebral disc degeneration by reprogramming cholesterol metabolism and inhibiting inflammatory signaling. *Acta Pharm Sin B* 2023;13(5):2269–80.
- [50] Qin T, Yan J, Li S, Lin X, Wu J, Huang Z, et al. MicroRNA-155 suppressed cholesterol-induced matrix degradation, pyroptosis and apoptosis by targeting ROR α in nucleus pulposus cells. *Cell Signal* 2023;107:110678.
- [51] Li Q, Zhao Y, Guo H, Li Q, Yan C, Li Y, et al. Impaired lipophagy induced-microglial lipid droplets accumulation contributes to the buildup of TREM1 in diabetes-associated cognitive impairment. *Autophagy* 2023;19(10):2639–56.
- [52] Yang Y, Li X, Liu Z, Ruan X, Wang H, Zhang Q, et al. Moderate treadmill exercise alleviates NAFLD by regulating the biogenesis and autophagy of lipid droplet. *Nutrients* 2022;14(22):4910.
- [53] Liu K, Qiu D, Liang X, Huang Y, Wang Y, Jia X, et al. Lipotoxicity-induced STING1 activation stimulates MTORC1 and restricts hepatic lipophagy. *Autophagy* 2022;18(4):860–76.
- [54] Zhang X, Wei M, Fan J, Yan W, Zha X, Song H, et al. Ischemia-induced upregulation of autophagy precludes dysfunctional lysosomal storage and associated synaptic impairments in neurons. *Autophagy* 2021;17(6):1519–42.
- [55] Cascajosa-Lira A, Prieto AI, Pichardo S, Jos A, Cameán AM. Protective effects of sulforaphane against toxic substances and contaminants: a systematic review. *Phytomedicine* 2024;130:155731.
- [56] Dinkova-Kostova AT, Fahey JW, Kostov RV, Kensler TW. KEAP1 and done? Targeting the NRF2 pathway with sulforaphane. *Trends Food Sci Technol* 2017;69(Pt B):257–69.
- [57] Lin H, Wang Y, Jing K, Wu T, Niu Y, Wei J. Nuclear factor erythroid-2 related factor 2 inhibits human disc nucleus pulposus cells apoptosis induced by excessive hydrogen peroxide. *Rev Assoc Med Bras* 1992;66(7):986–91. 2020.